Biochimica et Biophysica Acta 1848 (2015) 1646–1655

Contents lists available at ScienceDirect

Biochimica et Biophysica Acta

journal homepage: www.elsevier.com/locate/bbamem

The Parkinson-associated human P_{5B}-ATPase ATP13A2 protects against the iron-induced cytotoxicity

Débora E. Rinaldi, Gerardo R. Corradi, Lucía Martínez Cuesta, Hugo P. Adamo, Felicitas de Tezanos Pinto *

From IQUIFIB-Facultad de Farmacia y Bioquímica, Universidad de Buenos Aires, Junín 956, Buenos Aires 1113, Argentina

ARTICLE INFO

Article history:
Received 18 November 2014
Received in revised form 28 March 2015
Accepted 15 April 2015
Available online 23 April 2015

Keywords:
P-type ATPase
P_{5B}-ATP13A2
Iron
Lysosome membrane permeabilization
Parkinson disease

ABSTRACT

P-type ion pumps are membrane transporters that have been classified into five subfamilies termed P_1–P_5. The ion transported by the P_5-ATPases is not known. Five genes named *ATP13A1–ATP13A5* that belong to the P_5-ATPase group are present in humans. Loss-of-function mutations in the *ATP13A2* gene (PARK9, OMIM 610513) underlay a form of Parkinson's disease (PD) known as the Kufor–Rakeb syndrome (KRS), which belongs to the group of syndromes of neurodegeneration with brain iron accumulation (NBIA).
Here we report that the cytotoxicity induced by iron exposure was two-fold reduced in CHO cells stably expressing the ATP13A2 recombinant protein (ATP13A2). Moreover, the iron content in ATP13A2 cells was lower than control cells stably expressing an inactive mutant of ATP13A2. ATP13A2 expression caused an enlargement of lysosomes and late endosomes. ATP13A2 cells exhibited a reduced iron-induced lysosome membrane permeabilization (LMP). These results suggest that ATP13A2 overexpression improves the lysosome membrane integrity and protects against the iron-induced cell damage.

1. Introduction

P-type ATPases are characterized by the formation of a phosphorylated intermediate during their reaction cycle and are involved in the active transport of inorganic cations and other substrates across cell membranes. This superfamily is phylogenetically divided into five subfamilies termed P_1–P_5 or type I-V [1]. The P_5 subfamily is expressed only in eukaryotes and their substrate specificity is not known [2,3]. In humans, there were identified five genes named *ATP13A1–ATP13A5* that belong to this group of P_5-ATPases [3]. Two P_5-ATPases named Cod1p (or Spf1p) and Ypk9p were found in the yeast *Saccharomyces cerevisiae*. By DNA sequence alignment, it was shown that this type V ATPases must be divided in two groups named P_{5A} and P_{5B}; the mouse gene *Atp13a1* and the yeast gene coding Cod1p (*Yel031w*) are members of the first group, while the mouse genes *Atp13a2–Atp13a5* and the yeast gene coding Ypk9p (*Yor291w*) are clustered into the second one (1). P_{5A}-ATPases have been identified in the endoplasmic reticulum and seem to have basic functions in protein maturation and secretion, while P_{5B} ATPases localize to vacuolar/lysosomal or apical membranes and in animals play a role in hereditary neuronal diseases [4–7]. Loss-of-function mutations of the human gene *ATP13A2* were found to underlie an autosomal recessive form of early-onset parkinsonism (Kufor–Rakeb Syndrome) [6], which was recently proposed to be a type of neurodegeneration with brain iron accumulation (NBIA) [8,9].

Iron cycles easily between oxidized ferric Fe(III) and reduced ferrous Fe(II) and readily forms complexes with oxygen, making this metal a central player in respiration and related redox processes. However, free or redox-active iron is also associated with harmful processes because Fe(II) can react with oxygen (O_2) to form superoxide ($O_2^{\bullet-}$). More importantly, Fe(II) can also homolytically cleave hydrogen peroxide (H_2O_2) yielding hydroxyl radicals ($HO^{\bullet}$) and hydroxyl ions (OH^-) (Fenton-type reaction). $HO^{\bullet}$ is a particularly aggressive, oxidative, and short-lived species that reacts directly where it is formed. Superoxide is not a powerful oxidant but has the capacity to reduce Fe (III) to Fe(II), thereby initiating the production of the much more destructive $HO^{\bullet}$. Inside the lysosomal compartment, redox-active iron is formed when liberated following autophagic degradation, creating Fenton-type reactions with hydrogen peroxide that may diffuse from the cytosol. As a consequence, lysosome membrane may be destabilized by peroxidation of adjacent lipids or accumulate the age pigment lipofuscin with depression of autophagic capacity [10,11]. This damage is lessened by intralysosomal mechanisms that keep iron in bound form.

In this paper, we have investigated the sensitivity to $FeCl_3$ of CHO cells expressing the human P_{5B}-ATP13A2 wild type *(ATP13A2)* or a mutant in which the catalytic residue Asp 508 was substituted by Asn (*ATP13A2-D508N*) [12–14]. As expected, CHO cells mortality increased with increasing concentrations of $FeCl_3$; however, we found that the cytotoxic effect was reduced in the cells expressing the active ATP13A2 in

Abbreviations: CHO cells, Chinese hamster ovary cells; FCS, fetal calf serum; MTT, 3-(4,5-dimethyl-2-thiazolyl)-2,5-diphenyl-2H-tetrazolium bromide

* Corresponding author. Tel.: +54 11 49648289 147; fax: +54 11 4962 5457.
E-mail addresses: hpadamo@qb.ffyb.uba.ar (H.P. Adamo), ftpinto@qb.ffyb.uba.ar (F. de Tezanos Pinto).

http://dx.doi.org/10.1016/j.bbamem.2015.04.008
0005-2736/

conjunction with lower iron content. ATP13A2 expression caused an enlargement of lysosomes and late endosomes and increased the stability of lysosomes membranes toward the iron-induced permeabilization. These results support the idea that the expression of ATP13A2 protects CHO cells from iron-induced damage by stabilizing the lysosome integrity.

2. Materials and methods

2.1. Materials

Reagents were purchased from Life Technologies, and reagents for cell culture, dithiothreitol (DTT), ferric chloride ($FeCl_3$), phenylmethanesulfonyl fluoride (PMSF), chloroquine (CQ), *N*-acetyl-cysteine (NAC), and other chemicals, Sigma.

2.2. Cell culture and protein expression

Stable CHO cell lines transfected with the empty vector (pcDNA3.1) or expressing the recombinants human ATP13A2 (*ATP13A2*) or mutant ATP13A2-D508N (*ATP13A2-D508N*) were described previously [12–14]. The detection of the recombinant proteins was performed by immunoblotting using the antibody to ATP13A2 (Sigma). The cells were maintained in Dulbecco's modified Eagle medium supplemented with 0.1 mM hypoxanthine, 0.01 mM thymidine, 300 μg/ml geneticin (G418), 100 U/ml penicillin, 100 μg/ml streptomycin, and 10% fetal calf serum (FCS). The cells were grown in humidified 5% CO_2/air on standard plastic culture dishes.

2.3. Cell viability assay

CHO cells (2×10^4/well in 100 μl) were plated in 96-well microplates and incubated in the mentioned conditions. The medium was removed 24–48 h later, and the cells were washed and incubated in complete medium with increasing concentrations of $FeCl_3$, or with 1.5 mM $FeCl_3$ plus 0 or 5 mM *N*-acetyl-cysteine (NAC). The viability assay was performed the following day by measuring the activity of the lysosome enzyme β-hexosaminidase as described previously [13–15]. Because β-hexosaminidase is a lysosomal enzyme and its activity could be affected by the expression of the ATP13A2 protein in the same organelle, we validated our viability results also using the MTT (Sigma) assay.

2.4. Cell iron measurement

Cell iron content was measured quantitatively by the colorimetric ferrozine-based assay [16] and qualitatively by Perls' Prussian blue stain [17]. For the first method, CHO cells were seeded in 24-well culture plates with initial density of 5×10^4 cells per well and grown for 48 h as mentioned. The cells were washed twice with Hank's solution and incubated in complete medium with increasing concentrations of $FeCl_3$ for 24 h. Iron accumulation was terminated by washing the cells three times with 2 mL of ice-cold PBS. After completely removing the PBS, the cells were frozen and the dishes were stored at −20 °C. Cells were lysed with 200 μl of 50 mM NaOH for 2 h on a shaker in a humidified atmosphere. Aliquots (100 μl) of cell lysates were placed in Eppendorf tubes and mixed with 100 μl of 10 mM HCl (the solvent of the iron standard $FeCl_3$) and 100 μl of the iron-releasing reagent (a freshly mixed solution of equal volumes of 1.4 M HCl and 4.5% (w/v) $KMnO_4$ in H_2O). These mixtures were incubated for 2 h at 60 °C within a fume hood since chlorine gas is produced during the reaction. The HCl/KMnO4 pretreatment is sufficient to release iron quantitatively from proteins, including the iron-storage protein ferritin, and heme proteins such as hemoglobin. After the mixtures had cooled to room temperature, 30 μl of the iron-detection reagent (6.5 mM ferrozine, 6.5 mM neocuproine, 2.5 M ammonium acetate, and 1 M ascorbic acid dissolved in water) was added to each tube. After 30 min, 280 μl of the solution in each tube was transferred into a well of a 96-well plate, and the absorbance was measured at 550 nm in a Microplate Reader Model 2100C (Rayto, Shenzhen, China). The iron content of the sample was calculated by comparing its absorbance to that of a range of standard concentrations of equal volume that had been prepared in a way similar to that of the sample (mixture of 100 μl of $FeCl_3$ standards (0–300 μM) in 10 mM HCl, 100 μl 50 mM NaOH, 100 μl releasing reagent, and 30 μl detection reagent). The intracellular iron concentration determined for each well of a cell culture was normalized against the protein content of that well. For this purpose, aliquots (5–20 μl) of the cell lysate were transferred to 96-well microplates for protein determination by means of the Bio-Rad protein assay, with bovine serum albumin as a standard. The total iron content was expressed as nmol of iron per milligram of protein.

For Perls' staining, cells were plated (6×105 cells per well) on glass coverslips and cultured as mentioned. After 48 h, they were incubated in complete DMEM with 0.3 mM $FeCl_3$. Iron exposure was terminated 24 h later by washing the cells twice with 1 mL of ice-cold PBS. The cells were then fixed with 4% paraformaldehyde in PBS, washed twice with H_2O, incubated in Perls' staining solution (comprising equal parts of potassium ferrocyanide and HCl), washed 3 times with H_2O, counterstained with Neutral Red (Sigma), dehydrated, cleared in xylene, mounted using Dako Faramount Aqueous Mounting Medium, and observed by light microscopy (Lieca DM2000, Microsystems, Wetzlar, Germany).

2.5. Cytosol fraction isolation

CHO cells were plated (2×10^6 cells/well in 10 ml) in 100 × 20 mm cell culture dishes and incubated in the mentioned conditions. When the cells reached confluence the medium was removed, the cells were washed twice with PBS and resuspended in PBS-EDTA 1 mM by scraping. The cells were pelleted by centrifugation (10000×*g* for 15 min at 4 °C) and homogenized in 3 ml of isotonic solution containing Tris–HCl 10 mM (pH 7.4), KCl 0.15 M, 1 mM $MgCl_2$, 0.25 M sucrose and the protease inhibitors phenylmethanesulfonyl fluoride (PMSF) 0.1 mM, aprotinin 8 μg/ml and leupeptin 1 μg/ml. The homogenate was centrifuged at 12000×*g* for 10 min at 4 °C. The supernatant was transferred to a new tube and centrifuged at 25000×*g* for 15 min at 4 °C to precipitate the mitochondrial fraction. The supernatant was frozen in aliquots at −80 °C and used as the isolated cytosol fraction for the determination of the β-hexosaminidase activity. Protein concentration was estimated by means of the Bio-Rad protein assay, with bovine serum albumin as a standard.

2.6. Fluorescence microscopy with acridine orange (AO)

The staining of the cells with AO for the fluorescence microscopy assays was described previously [13]. Briefly, the cells were cultured on glass multiwell plates for 48–72 h, washed with PBS, and incubated with the pH-sensitive fluorescent dye AO (Sigma) 0.05 μM for 10 min. The cells were then washed, and the living cells were directly observed by confocal microscopy (FluoView 1000, Olympus, Japan) with an appropriate AO filter. The digitized images were analyzed by using the ImageJ Software program (NIH) to measure the mean vesicle area of each image. Briefly, the threshold was adjusted to take off the background and establish the lower fluorescence limit detection; this parameter was the same for all the analyzed images. Finally, the Analyze Particles routine of ImageJ was used, and the output table with the number and size of the vesicles was analyzed with Excel. Values are expressed as the mean vesicle area obtained for each cell type. In each case, at least 50 cells from three or four independent experiments were scored.

2.7. Electron microscopy

Cells were fixed in 0.1 M sodium cacodylate trihydrate (pH 7.5) for 24 h. Then they were postfixed with 1.5% OsO_4 and embedded in Spurr resin after dehydration. Ultrathin sections (60 nm) were cut with an ultramicrotome. The specimens were examined with a Zeiss EM 109 T electron microscope, 80 kV (Zeiss Inc, Oberkochen, Germany); images were acquired with a Gatan ES1000W (11Megapixel) camera.

2.8. Lysosomal membrane permeability assays

Cells were assessed for lysosomal stability using the AO uptake and relocation methods [18] and the cytoplasmic presence of the lysosomal enzyme β-hexosaminidase [15].

2.8.1. The AO method

AO is a lysosomotropic base and a metachromatic fluorochrome exhibiting red fluorescence when highly concentrated (as is the case in intact lysosomes where AO is retained in its charged, AOH^+, form). And green fluorescence at low concentration (as is the case when some lysosomes have ruptured and AO relocates to the cytosol where it occurs predominantly in the deprotonated form). The remaining intact lysosomes were evaluated by assaying the red fluorescence (AO uptake method). However, because of the much higher sensitivity of the photomultiplier to green than to red photons, this method is less sensitive than following AO relocation within cells stained with AO (AO relocation method). In some cases, early and minor lysosomal destabilization were detected by the AO relocation method, while the AO uptake method was observed in later and more pronounced lysosomal rupture. CHO cells stably expressing the recombinants ATP13A2 or ATP13A2-D508N pumps (8×10^4/well in 100 μl) were plated in 96-well microplates and incubated in the mentioned conditions. After 48 h, the cells were exposed to 0.3 or 1.5 mM $FeCl_3$ in complete growth medium for 24 h or 1.5 h, respectively. Following $FeCl_3$ treatment, AO 5 μg/ml was added and incubated for 10 min at 37 °C in the dark. The cells were then washed three times with 200 μl PBS, 100 μl of complete DMEM was added to the living cells and where then directly observed by confocal microscopy (FluoView 1000, Olympus, Japan). The excitation wavelength was 473 nm, and the green and red fluorescence emissions were recorded between 509-562 nm and 630-693 nm, respectively. For the enhance oxidative stress assay, the cells were incubated with 0.3 mM $FeCl_3$ in complete growth medium for 24 h, and 1.5 or 3 mM H_2O_2 was added to the culture for 1 h before being stained with AO as mentioned before.

For image quantification, the digitized images were analyzed by using the ImageJ Software program (NIH) to measure the mean red fluorescence intensity of all vesicles of each cell or the mean green fluorescence intensity of the whole cell. In each case, at least 20 cells from four independent experiments were scored.

2.8.2. β-Hexosaminidase enzymatic assay

For the detection of the lysosomal enzyme β-hexosaminidase in the cytosol, the cells were incubated with 1.5 mM $FeCl_3$ for 1.5 h because we obtained similar results as that observed by incubating with 0.3 mM FeCl3 for 24 h when using the AO method. The cells were then rinsed extensively with PBS and removed by scraping in the homogenization buffer. The cytosolic fraction was isolated as described above. Fifty microliters of the isolated cytosol fraction was incubated with 60 μl substrate solution (7.5 mM *p*-nitrophenol-*N*-acetyl-beta-D-glucosaminide (Sigma), 0.1 M sodium citrate pH 5.0, and 0.25% Triton X-100) at 37 °C with 100% humidity for 4 h. The colorimetric product was visualized by adding 90 μl developer solution (50 mM glycine pH 10.4, 5 mM EDTA) and quantified by recording the absorbance at 405 nm in a Microplate Reader Model 550 (Bio-Rad, Tokyo, Japan). β-hexosaminidase activity was measured in duplicate. We normalized the activity of the lysosomal enzyme by correcting the activity in the cytosol of $FeCl_3$ treated cells with the activity of untreated cells used as control.

2.9. Fluorescence imaging of F-actin cytoskeleton

Cells were plated (6×10^5) on glass coverslips and incubated in the mentioned conditions. After 48 h, they were incubated with 1.5 mM $FeCl_3$ for 1.5 h at 37 °C. The cells were then fixed with 4% paraformaldehyde in PBS for 10 min, permeabilized with 0.1% Triton X-100 in PBS for 10 min, washed three times with PBS, and incubated with 1 μg of Phalloidin-TRITC conjugate (Sigma) per ml in PBS. Nuclei were stained with 2.5 μM Hoechst 33258. Each coverslip was mounted in SouthernBiotech Fluoromount-G™ Slide Mounting Medium and observed by confocal microscopy (FluoView 1000, Olympus, Japan) with an appropriate TRITC filter.

3. Results

3.1. ATP13A2-expressing cells are more resistant to $FeCl_3$ treatment

The effect of $FeCl_3$ on the viability of control CHO cells transfected with the empty vector (pcDNA3.1), and cells expressing ATP13A2 or the inactive mutant ATP13A2-D508N was investigated by measuring the activity of the endogenous enzyme β-hexosaminidase. We have previously shown that the recombinant proteins were expressed at similar levels [13,14]; see Supplemental Fig. 1, available on the website for more details. Fig. 1a shows the viability of CHO cells incubated for 24 h with increasing concentrations of $FeCl_3$; as expected, the metal exerts a dose-dependent cytotoxic effect. The exposure to 1 mM $FeCl_3$ reduced the viability of CHO cells transfected with the empty vector (pcDNA3.1) or expressing the ATP13A2-D508N at less than 60%. Under the same conditions, near 90% of ATP13A2 cells remained viable, indicating that the expression of ATP13A2 made the cells more resistant to iron treatment than CHO cells transfected with the empty vector or expressing the ATP13A2-D508N mutant pump. Similar results were obtained by measuring the viability with the MTT method (data not shown).

Since the toxic effect of iron is presumably related to oxidative stress, CHO cells were treated with FeCl3 plus the antioxidant NAC. As depicted in Fig. 1b, NAC protected the cells from the cytotoxic effect of iron exposure.

3.2. Iron depositions are reduced in ATP13A2-expressing CHO cells

Because an accumulation of intracellular iron may induce cell death by the generation of reactive oxygen species (ROS) through Fenton-type reactions, we measured the iron content of CHO cells by the ferrozine method. As shown in Fig. 2a, the iron accumulation increased gradually with increasing concentrations of $FeCl_3$ after 24 h treatment. ATP13A2-D508N cells showed higher iron content than ATP13A2 cells at all $FeCl_3$-tested concentrations. This increment in the iron content in ATP13A2-D508N cells varied from 20 to 55%, depending on the amount of $FeCl_3$ added to the culture medium. Higher $FeCl_3$ concentrations could not be tested because of the insoluble precipitates formed by iron in the presence of FCS.

The results were confirmed by Perls' Prussian blue stain. In this method, iron reacts with potassium ferrocyanide to form ferric ferrocyanide, the intensity of this insoluble, blue compound indicates qualitatively the iron amount. A non-toxic $FeCl_3$ concentration was used in order to minimize cell mortality and analyze an equal cell number in each field. As shown in Fig. 2b, control cells not exposed to $FeCl_3$ show no blue depositions. In contrast, insoluble blue sediments were observed in cells exposed to 0.3 mM $FeCl_3$ for 24 h. The intensity of the blue precipitate was clearly much higher in pcDNA3.1 and ATP13A2-D508N cells than in ATP13A2 cells.

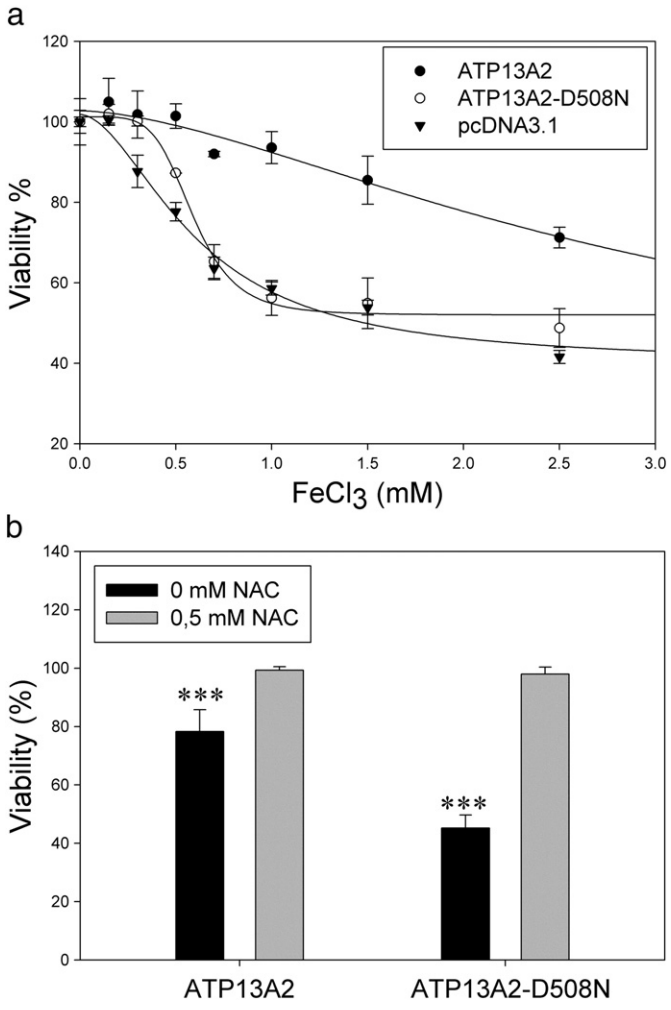

Fig. 1. Viability of CHO cells transfected with the empty vector (pcDNA3.1) or stably expressing the ATP13A2 (*ATP13A2*) or ATP13A2-D508N (*ATP13A2-D508N*) pumps. (a) The cells were incubated for 24 h at 37 °C with increasing concentrations of ferric chloride ($FeCl_3$). The viability assay was performed by measuring the activity of the endogenous enzyme β-hexosaminidase as described in Section 2. Values are expressed as the percentage of the absorbance at 405 nm measured for untreated cells. Data are shown as means ± SEM of 4 independent experiments done by sextuplicate. The line represents the best fit to the data given by the following equation: viability = min + (max − min) / [1 + ($FeCl_3$/EC50)$^{-Hillslope}$] (with min ≥ 0); with ATP13A2: min = 30 ± 135%, max = 102 ± 3%, EC50 = 2.95 ± 6.03 mM, hillslope = 1.6 ± 1.3; ATP13A2-D508N: min = 52 ± 2%, max = 101 ± 1%, EC50 = 0.59 ± 0.02 mM, hillslope = 5.3 ± 0.9; pcDNA3.1: min = 39 ± 6%, max = 101 ± 3%, EC50 = 0.61 ± 0.09 mM, hillslope = 1.8 ± 0.4. (b) Cells were treated as in "a" with 1.5 mM $FeCl_3$ plus 0 or 5 mM NAC for 24 h. The viability assay was performed as mentioned before. A representative experiment from four independent experiments is shown where each point is the mean ± SD of quadruplicate determinations (***$p < 0.001$, significantly different from NAC-treated cells). Statistical significance was assessed by one-way analysis of variance (ANOVA) followed by Bonferroni post tests (GraphPad Prism 4, GraphPad Software, Inc.).

3.3. Enlargement of acidic vesicles by the overexpression of the P_{5B}-ATPase ATP13A2

It has been shown that ATP13A2 co-localizes with intracellular acidic compartments, particularly lysosomes and endosomes [19], and that the deficiency of ATP13A2 leads to lysosomal dysfunction [20,21]. The lysosomal compartment consists of a large number of vacuoles with a pronounced fusion and fission activity [22], and the lysosome degradation pathway inhibition alters iron metabolism and transport [11,23]. We evaluated the size of acidic vesicles by staining CHO cells with the lysosomotropic agent AO. The autofluorescent dye AO accumulates mainly in the acidic vacuolar apparatus due to proton trapping. Fig. 3a shows that larger vesicles were observed in ATP13A2-expressing cells when stained with AO. The image analysis indicated that the average size of the acidic vesicles of ATP13A2 cells was 2-fold larger than those from ATP13A2-D508N cells (Fig. 3b). This observation was also confirmed by electron microscopy (Fig. 3d). Strikingly, the observed vesicles in ATP13A2-expressing cells were not only larger but also showed more electron dense bodies resembling late autophagic vacuoles-like structures [24].

The effect of the inhibitor of the intralysosomal catabolism chloroquine (CQ) was investigated. CQ is a known lysosomotropic agent that increases lysosomal pH by accumulating within lysosomes as a deprotonated weak base. CQ induces the dilation of lysosomes and the accumulation of lipid bodies that may represent intracellular debris as a consequence of dysfunctional lysosomes [25,26]. Besides, the dilation of these vesicles allows us to observe them as individual entities. Fig. 3a shows CHO cells exposed to 0.2 mM CQ for 2 h and stained with 0.05 μM AO. As expected, CQ treatment caused the dilation of the acidic vesicles, but this increment was similar for ATP13A2 and ATP13A2-D508N cells (Fig. 3c), showing that the acidic vesicles are larger in ATP13A2 cells even in CQ absence.

3.4. Iron-induced lysosome membrane permeabilization (LMP) is reduced in ATP13A2-expressing CHO cells

The production of highly reactive hydroxyl radicals from H_2O_2 by intralysosomal iron-catalyzed Fenton-type reactions induces LMP through lysosome membrane lipid peroxidation as one of the first events induced by iron overload [23,27–31]. Because ATP13A2 is expressed in the membrane of this organelle, we hypothesized that this enzyme may affect this process. Consequently, we investigated the iron-induced LMP in CHO cells by assessing the changes in green and red fluorescence of cells stained with AO before and after the exposure to $FeCl_3$, respectively. Due to its metachromatic properties, AO emits red fluorescence inside the lysosomes, where it is highly concentrated, and emits weakly green fluorescence in the cytosol and nucleus, where its concentration is lower. Consequently, an increased cytosolic green fluorescence, due to AO leak from damaged lysosomes and a decline in red fluorescence from lysosomes are markers of the loss of lysosomal membrane integrity. We used a relative low iron concentration of 0.3 mM that minimally affects viability in order to detect subtle changes in membrane permeability which characterizes the initial steps of the iron cytotoxic process. Fig. 4a shows ATP13A2 or ATP13A2-D508N cells stained with AO after $FeCl_3$ exposure. An increase in green fluorescence (Fig. 4b) and a decreased in red fluorescence (Fig. 4c) is observed when AO is released from lysosomes into the cytosol due to iron treatment. By comparison of figures obtained from ATP13A2 or ATP13A2-D508N cells, it can be seen that the iron-induced LMP was greater in ATP13A2-D508N cells than in ATP13A2 cells. The protection from the iron-induced LMP conferred from ATP13A2 expression was independently confirmed by measuring the activity of the lysosome-resident β-hexosaminidase released in the cytosol fraction from permeabilized lysosomes. Fig. 4d shows the β-hexosaminidase activity of the cytosolic fraction isolated from ATP13A2 and ATP13A2-D508N of $FeCl_3$-treated cells. The lysosome-resident enzyme activity was about 30% lower in cells expressing ATP13A2 compared with those expressing ATP13A2-D508N.

Since intralysosomal iron-catalyzed oxidative processes led to lysosomal rupture [32], we further challenged the iron-protection exerted by ATP13A2 expression by using a free radical generator, such as hydrogen peroxide. To test this, we treated CHO cells overexpressing the recombinant proteins for 24 h with 0.3 mM $FeCl_3$ and 1.5 or 3 mM H_2O_2 was added to the culture medium for 1 h before the AO staining as described before. As shown in Fig. 4c, the treatment of CHO cells with $FeCl_3$ plus H_2O_2 further decreased the red punctuate fluorescence in a concentration dependent manner (see Fig. 4b, right panels with 1.5 and 3 mM H_2O_2). Nevertheless, by comparison of panels showing CHO cells treated with $FeCl_3$ plus 1.5 mM H_2O_2, ATP13A2-expressing cells were

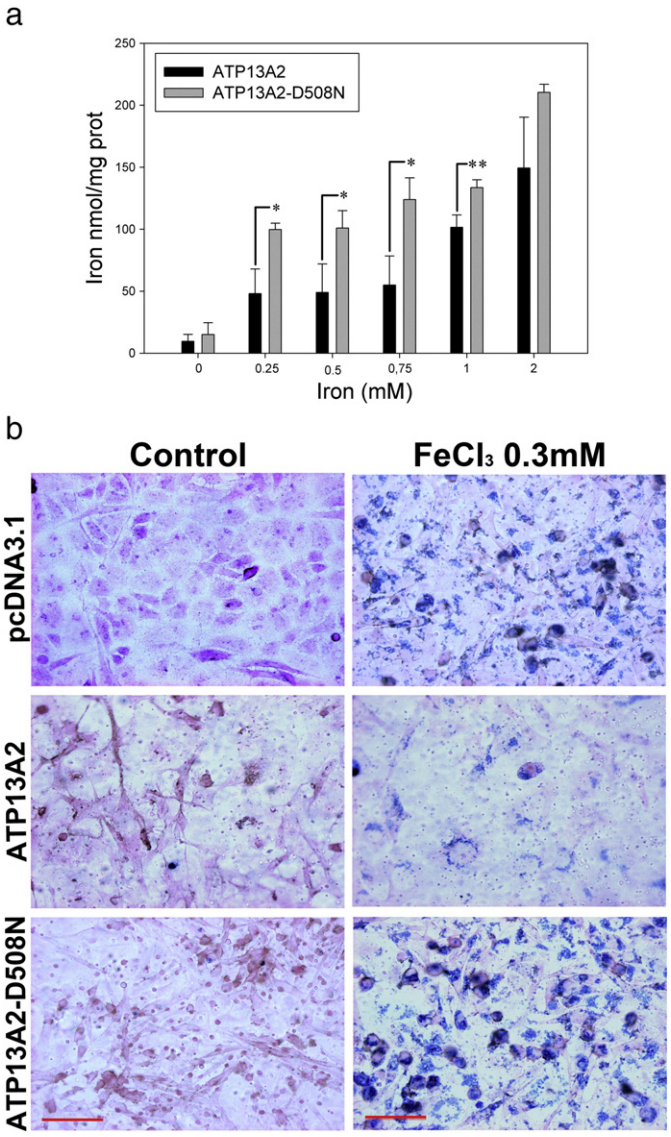

Fig. 2. Iron content measurement of *ATP13A2* and *ATP13A2-D508N* cells. The cells were treated with the indicated $FeCl_3$ concentrations for 24 h, and the iron accumulation was measured by (a) the colorimetric ferrozine-based assay or by (b) Perls' Prussian Blue staining (blue, iron stain; pink, nuclear–cytoplasmic counterstain). CHO cells transfected with the empty vector (pcDNA3.1) were included as another control. Bar, 50 μm. A representative experiment from three independent experiments is shown in "a" where each point is the mean ± SD of triplicate determinations. $^{**}p < 0.01$ and $^{*}p < 0.1$ significantly different from ATP13A2-expressing CHO cells (Student's *t* test, GraphPad Prism 4, GraphPad Software, Inc.).

less affected, as can be seen by the lower decrease of the red punctuate fluorescence. Accordingly, ATP13A2-D508N cells were more susceptible to the damaging effect of $FeCl_3$ and 3 mM H_2O_2 as suggested by the almost imperceptible "punctuate" red fluorescence and the gain in cytoplasmic red fluorescence denoting the loss of lysosomal integrity.

3.5. ATP13A2 expression protects against the iron-induced actin cytoskeleton remodeling

Cathepsins, hydrolases, H^+, and Ca^{2+} [28,31,33] can escape into the cytosol as a consequence of LMP. The leakage of lysosome content leads to actin cytoskeleton reorganization [34]. The ability of iron to stimulate the reorganization of actin in CHO cells was assessed by fluorescence microscopy of F-actin stained with Phalloidin-TRITC conjugate (Sigma). As shown in Fig. 5, untreated control cells had typical cellular morphology with a well-defined actin cytoskeleton. In contrast, ATP13A2-D508N cells became rounded and exhibited a less organized actin cytoskeleton after $FeCl_3$ treatment. Noteworthy, in ATP13A2 cells, the iron-induced changes in the actin cytoskeleton were almost undetectable.

4. Discussion

Iron is found in high concentration in some areas of the brain, and increased accumulation of iron in the substantia nigra is a feature of PD. KRS is a form of Parkinson due to ATP13A2 gene mutations, which was recently included in the group of syndromes of neurodegeneration with brain iron accumulation (NBIA) [9]. Here we report that the overexpression of a functional ATP13A2 makes CHO cells more resistant to $FeCl_3$ exposure. Accordingly, the increase of iron depositions due to $FeCl_3$ treatment was diminished by ATP13A2 expression.

Lysosomes engaged in degrading iron-rich compounds are rich in potentially redox-active iron, while resting lysosomes may contain no iron at all. These iron-rich lysosomes are sensitive to oxidative stress, and the magnitude of oxidative stress determines the degree of lysosomal destabilization and, consequently, whether arrested growth, reparative autophagy, apoptosis, or necrosis will follow. Namely, there is a range in the iron level which can be handled by the cells before triggering the cell death pathways, but once the maximum iron level is overcome, the cell is indefectibly destined to die. Since iron overload

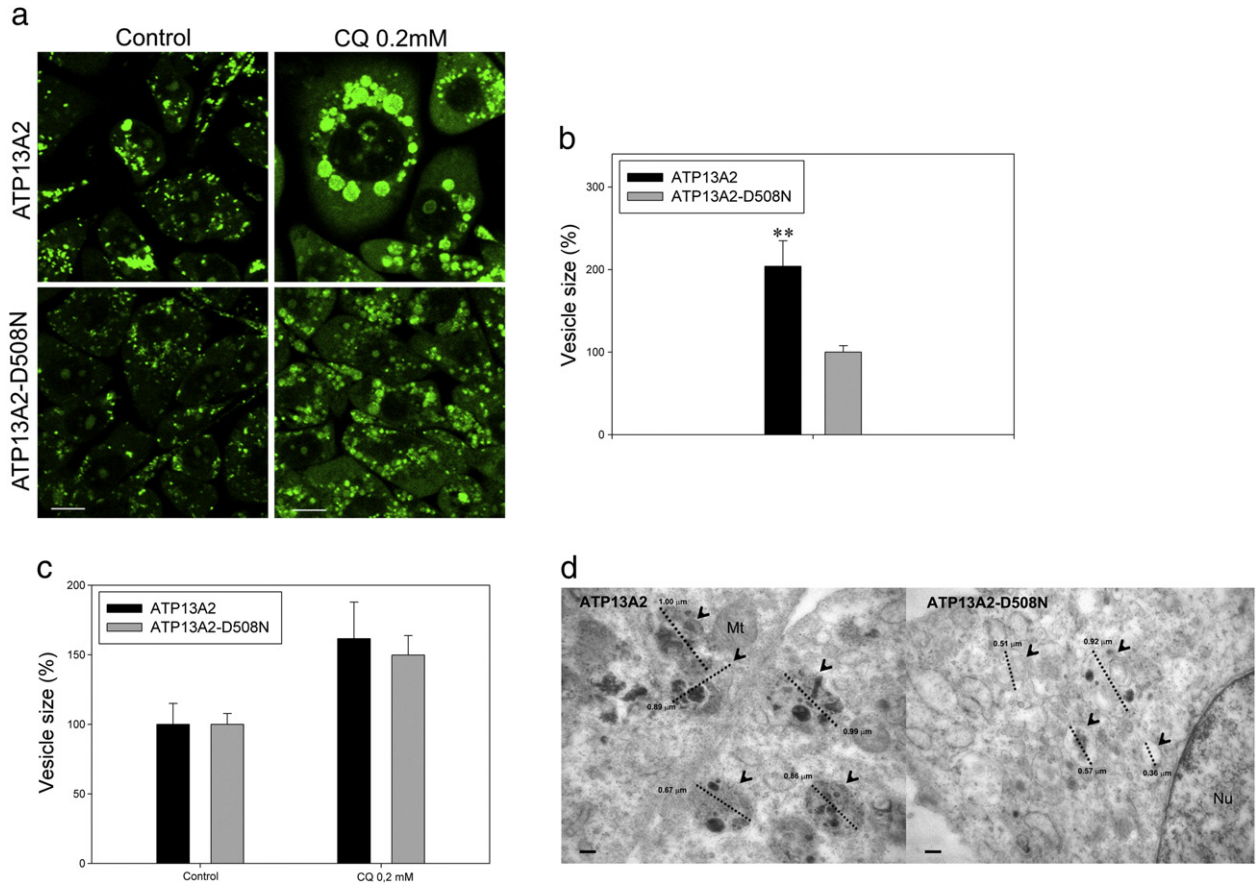

Fig. 3. Fluorescence microscopy of *ATP13A2* and *ATP13A2-D508N* cells stained with the lysosomotropic dye AO. (a) The cells were cultured on glass multiwell plates for 48 h and were then incubated with 0 or 0.2 mM CQ for 2 h at 37 °C before being stained with AO 0.05 μM. The living cells were directly observed by confocal microscopy (FluoView 1000, Olympus, Japan) with an appropriate AO filter. Bar, 10 μm. (b) Quantitative analysis of *ATP13A2* and *ATP13A2-D508N* cells stained with AO indicates the increased size of acidic vesicles due to ATP13A2 overexpression The vesicle size is expressed as the percentage of the mean vesicle area of ATP13A2-D508N cells ($0.83 \pm 0.06\ \mu M^2$) calculated by the ImageJ Software program. $^{**}p < 0.01$ significantly different from ATP13A2-D508N cells (Student's *t* test, GraphPad Prism 4, GraphPad Software, Inc.). (c) Quantitative analysis of ATP13A2 and ATP13A2-D508N cells treated with CQ 0.2 mM for 2 h at 37 °C before being stained with AO shows the increased size of acidic vesicles due to CQ exposure. The vesicle size is expressed as the percentage of the mean vesicle area obtained for each cell type without CQ exposure (ATP13A2 = $1.69 \pm 0.25\ \mu M^2$, ATP13A2-D508N = $0.83 \pm 0.06\ \mu M^2$) calculated by the ImageJ Software program. (d) Electron microscopic examination of CHO cells stably expressing ATP13A2 or ATP13A2-D508N. Note in ATP13A2-expressing cells the enlargement of autolysosome-like structures (arrowheads) that contain granular deposits. Mt, mitochondria; Nu, nucleus. Bar, 0.2 μm.

triggers many proapoptotic and antiapoptotic pathways, which finally determine the cell destiny, a non-linear correlation between iron accumulation and viability is feasible. In this line, our results show that ATP13A2 cells can better tolerate the iron overload under an iron range of 0.25 to 1 mM in the culture medium.

We have recently shown that the expression of the human P_{5B}-ATPase ATP13A2 increases spermidine uptake in CHO cells [14]. Due to their amino groups, polyamines like spermidine are able to chelate metallic cations such as iron [35,36] maintaining it in a non-redox-active form. Polyamine transport is initiated by an unidentified plasma membrane carrier, and it is rapidly followed by sequestration into acidic vesicles of the late endocytic compartment [37]. Thus, it can be conceived that ATP13A2 cells containing larger lysosomes equipped with more iron-chelating agents like polyamines are more efficient at preventing the LMP generated by iron-catalyzed Fenton reactions. Supporting this hypothesis, here we found that acidic vesicles are enlarged in ATP13A2-expressing CHO cells, and the iron-induced LMP was also reduced in these cells. Accordingly, it was recently demonstrated that the overexpression of ATP13A2 produces a marked increase in the diameter and number of autophagosomes [19], the primary double-membrane vacuoles that engraft cytoplasmic proteins and suborganelles, which are then fused to lysosomes for bulk degradation in autophagy. A tempting explanation is that ATP13A2 expression may promote the fusion of acidic vesicles promoting their size-increment. Favoring this idea, it was recently published that autophagosomes surrounded by ATP13A2 were observed when the later stage(s) of autophagy where inhibited [38]. This observation opens the possibility that the P-type ATPase may be involved in the fusion of these entities with lysosomes improving the autophagosomal flux. Also worth mentioning is the fact that spermine prevents iron accumulation and depress lipofuscin (age pigment) formation in cultures myocardial cells [39]. Lipofuscin is a non-degradable, iron-rich, autofluorescent, polymeric compound that slowly accumulates within age in long-lived postmitotic cells at a rate that inversely correlates with longevity [11,40]. Even under normal conditions, iron-catalyzed peroxidation takes place intralysosomally, resulting in the oxidative modification of the autophagocytosed material which becomes resistant to the hydrolytic activity of lysosomal enzymes. If cells do not divide, this material progressively accumulates within the lysosomal compartment in the form of lipofuscin inclusions [11]. A mutation of the ATP13A2 gene causes neuronal ceroid lipofuscinosis, which comprises a heterogeneous group of metabolic storage diseases that are characterized by the accumulation of lipofuscin, neurodegeneration, and premature death [41,42].

LMP is one of the first events induced by iron overload and this is followed by the release of cathepsins and other lysosome-resident enzymes from lysosomes which, depending on the magnitude of lysosomal rupture, triggers the apoptotic mechanism that leads to cell death [23,27]. Accordingly, here we show that the LMP induced by iron treatment evaluated by the AO relocation method or by measuring the activity of

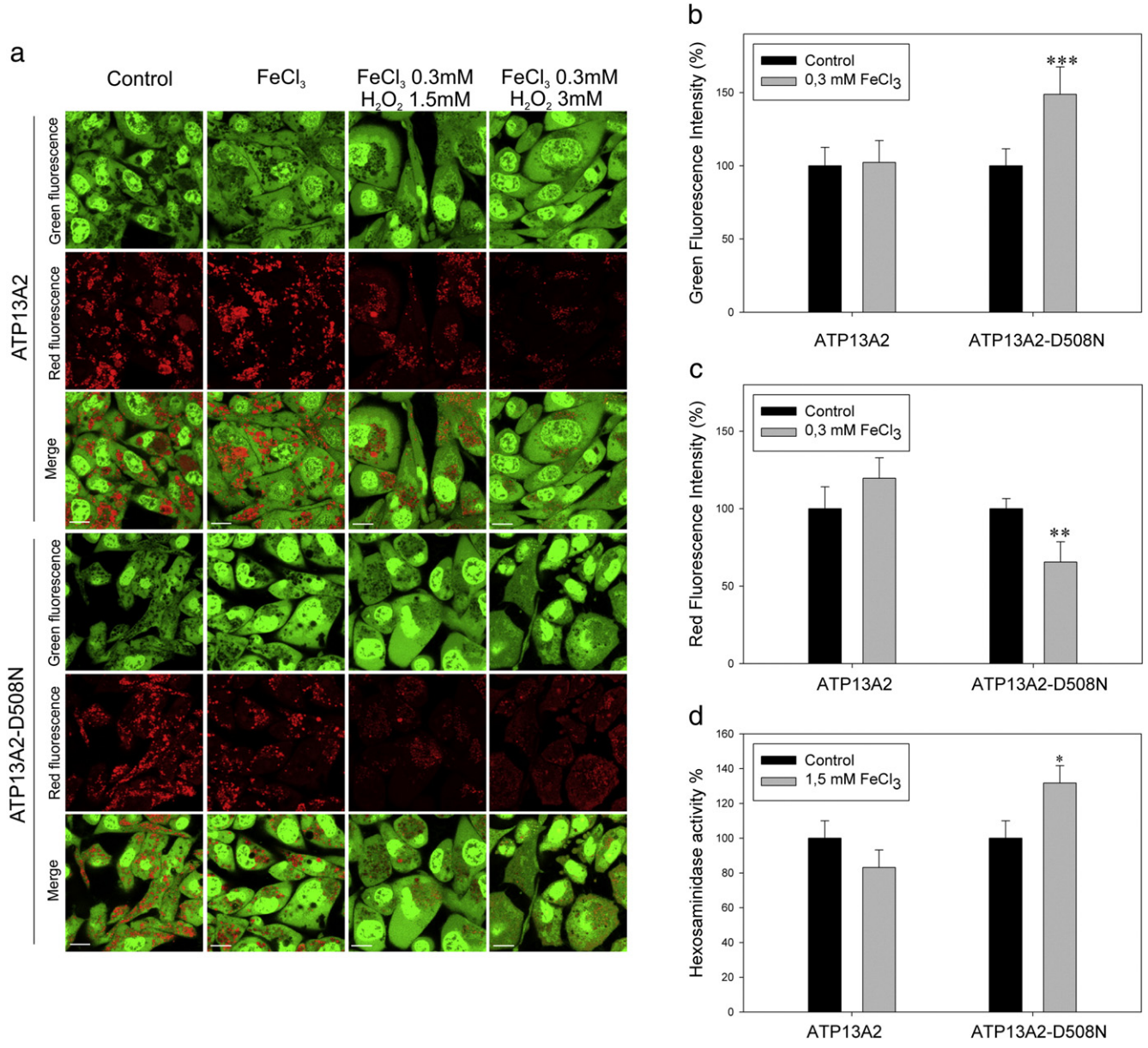

Fig. 4. Lysosome membrane permeabilization (LMP) detection by fluorescence microscopy in *ATP13A2* and *ATP13A2-D508N* cells. (a) Cell monolayers were incubated for 24 h at 37 °C with 0 or 0.3 mM $FeCl_3$ or plus 1.5 or 3 mM H_2O_2 for 1 h in complete DMEM and stained for 10 min with AO 5 μg/ml. After three washes in PBS, the living cells where excited at 473 nm, and the green and red fluorescence were directly observed by confocal microscopy (FluoView 1000, Olympus, Japan) as described in Section 2. Note the loss of the punctate red staining of acidic organelles and/or increase of green fluorescence after $FeCl_3$ treatment and gain of the cytoplasmic red fluorescence induced by H_2O_2 exposure in ATP13A2-D508N cells denoting the rupture of lysosome integrity. Bar, 10 μm. Quantitative image analyses of (b) green and (c) red fluorescence intensities. The fluorescence intensity is expressed as the percentage of the fluorescence intensity obtained for each cell type without iron exposure calculated by using the ImageJ Software program (NIH). $^{***}p < 0.001$ and $^{**}p < 0.01$ significantly different from untreated cells (Student's *t* test, GraphPad Prism 4, GraphPad Software, Inc.). (d) For the determination of the β-hexosaminidase activity of the cytosolic fraction, the cells were incubated for 1.5 h at 37 °C with 1.5 mM $FeCl_3$ in complete DMEM, and the activity was determined in 50 μl of the cytosol fraction as described in Section 2. Values are expressed as the percentage of the absorbance at 405 nm measured for untreated cells. A representative experiment of three independent experiments is shown, where each point is the mean ± SD of triplicate determinations. $^{*}p < 0.1$ significantly different from untreated cells (Student's *t* test, GraphPad Prism 4, GraphPad Software, Inc.).

the lysosome-resident β-hexosaminidase was reduced in ATP13A2 cells. An immediate event induced by the "lysosome content release" is the actin cytoskeleton reorganization [34]. The actin cytoskeleton plays a fundamental role in endocytosis and intracellular trafficking and is an essential component for the well-functioning of the lysosome degradation pathway. Interestingly, here we found that the expression of ATP13A2 also prevents the iron-induced actin cytoskeleton remodeling. This modification in the vesicle trafficking may explain the increased iron depositions observed in ATP13A2-D508N cells after 24 h exposure.

Earlier studies suggested the involvement of the P_5-ATPases in the homeostasis of Ca^{2+} [5,43,44], Mn^{2+} [45,46], Ni^{2+} [47] and most recently Zn^{2+} [38,48]. Interestingly, all these cations can be related to the development of PD [49–53], and the dysregulation of anyone of them may alter the other's level. Moreover, the P_5-ATPase associated dysfunction of intracellular membrane compartments like the ER, Golgi, and lysosome–endosome system could be either the cause or the consequence of metal ion dyshomeostasis. Keeping this in mind, the iron-protection induced by the expression of ATP13A2 could be exerted through modifications of the cation transport. Nevertheless, we found similar iron uptake or extrusion kinetics during the first 3 h in ATP13A2- or ATP13A2-D508N cells (data not shown). Hence, the ATP13A2 protection against iron exposure seems to be exerted through a mechanism that promotes the preservation of the lysosome integrity

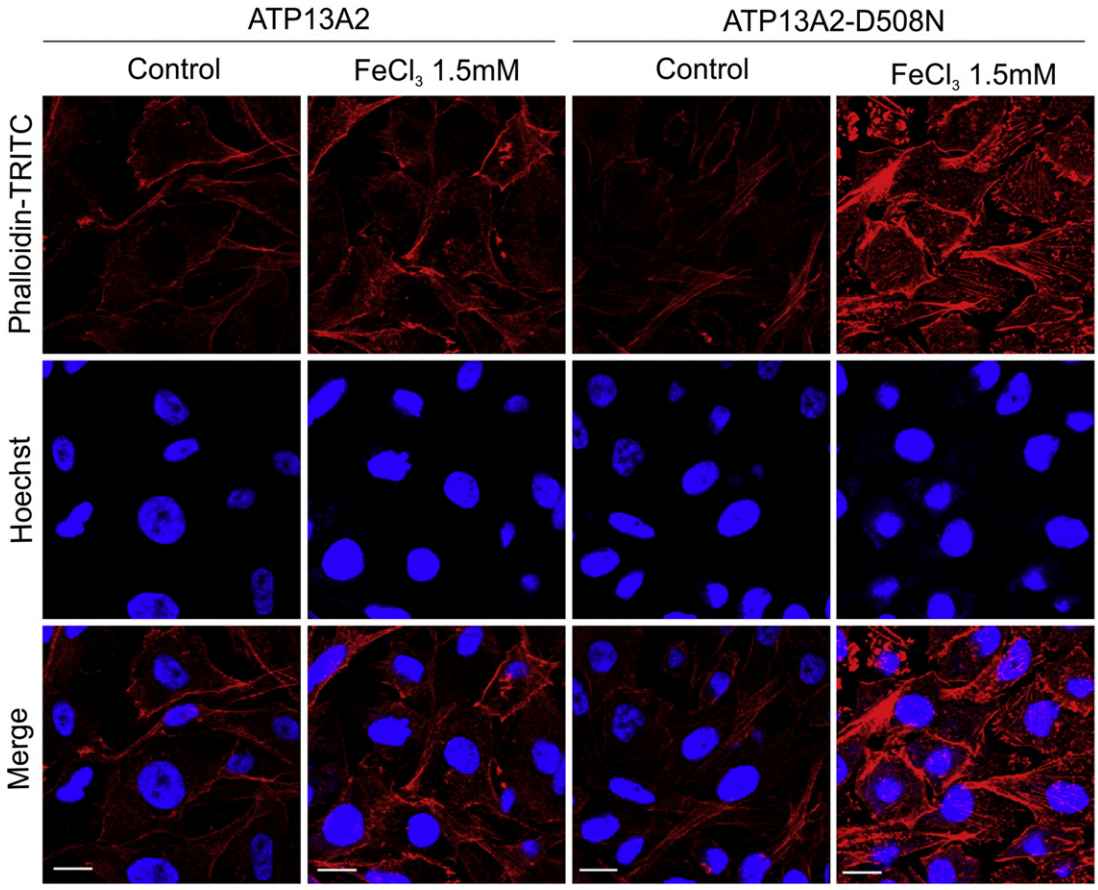

Fig. 5. Fluorescence microscopy of the F-actin cytoskeleton in *ATP13A2* and *ATP13A2-D508N* cells. The stably transfected cells were cultured on coverslips for 48 h. The cells were then incubated under basal conditions (left panels) or with 1.5 mM $FeCl_3$ (right panels) for 1.5 h at 37 °C. The F-actin cytoskeleton was stained with Phalloidin-TRITC (red), and the nucleus were stained with Hoechst (blue) as described in Section 2. Merge images are shown in lower panels. Bar, 10 μm.

against the known iron-induced lipid peroxidation rather than a modulation of the cation transport kinetic. In this line, non-raft domains enriched in phospholipids containing polyunsaturated fatty acids (PUFAs) and vitamin E are more sensitive to lipid peroxidation than lipid raft domains enriched in sphingolipids and cholesterol [54]. As the P-ATPases phylogenetically closest to the P5-ATPases are the P4-ATPase phospholipid transporters [55], it has been speculated that also the P5-ATPases may be involved in the active transport of lipids [56]. Since the proper content and distribution of phospholipids in the membrane is essential for the correct lysosome function, further experiments examining the details of the lysosome membrane composition of ATP13A2-expressing CHO cells may help to reach a better understanding of its role in lysosome membrane integrity.

Also worth mentioning is the fact that any change in lipid composition or distribution would modify the membrane functionality, altering not only all the processes mediated by the membrane bilayers but also the intra-organelle composition. Since manganese and zinc are able to induce LMP [57,58] and the homeostasis of these cations are also modified by ATP13A2 expression [38,45,46,48], we cannot exclude the possibility that the results shown here could be a general response to metals rather than an specific iron effect. However we did not observe any significant difference between control cells and those expressing the ATP13A2 pump in the viability of CHO cells treated with $MnCl_2$ [13]. Moreover, several contradictory results were reported with the same cations in different expression systems [57]. Further experiments will help to evaluate the possible involvement of ATP13A2 in the response to general osmolarity changes.

Supplementary data to this article can be found online at http://dx.doi.org/10.1016/j.bbamem.2015.04.008.

Transparency document

The Transparency Document associated with this article can be found, in the online version.

Author contribution

Debora E. Rinaldi, Gerardo R. Corradi, Lucía Martínez Cuesta, and Felicitas de Tezanos Pinto performed all experimental work and interpreted results. Hugo P. Adamo and Felicitas de Tezanos Pinto designed research and wrote the paper.

Funding

This work was supported by the University of Buenos Aires [UBA, grant no. B604], the Consejo Nacional de Investigaciones Científicas y Técnicas [CONICET, grant no. PIP 112-200801-02022], and the Agencia Nacional de Promoción Científica y Tecnológica [ANPCyT, grant nos. BID PICT 2007-702, 2011-2347, and 2013-1240].

Acknowledgements

We thank Dr Alfredo Ramirez, Dr Christian Kubisch (Institute of Human Genetics, University of Bonn, Germany), Dr Peter Vangheluwe, and Dr Tine Holemans (Faculty of Medicine, Department of Molecular Cell Biology, University of Leuven, Belgium) for supplying vectors pcDNA3.1 carrying the human ATP13A2 and ATP13A2-D508N cDNAs. We also thank Margarita Lopez from the National Research Laboratory and Electronic Microscopy Services (LANAIS-MIE) for the technical assistance.

References

[1] K.B. Axelsen, M.G. Palmgren, Evolution of substrate specificities in the P-type ATPase superfamily, J. Mol. Evol. 46 (1998) 84–101.
[2] A.B. Møller, T. Asp, P. Bach Holm, M.G. Palmgren, Phylogenetic analysis of P5 P-type ATPases, an eukaryotic lineage of secretory pathway pumps, Mol. Phylogenet. Evol. 46 (2007) 619–634.
[3] P.J. Schultheis, T.T. Hagen, K.K. O'Toole, A. Tachibana, C.R. Burke, D.L. McGill, G.W. Okunade, G.E. Shull, Characterization of the P5 subfamily of P-type transport ATPases in mice, Biochem. Biophys. Res. Commun. 323 (2004) 731–738.
[4] A. Di Fonzo, H.F. Chien, M. Socal, S. Giraudo, C. Tassorelli, G. Iliceto, G. Fabbrini, R. Marconi, E. Fincati, G. Abbruzzese, P. Marini, F. Squitieri, M.W. Horstink, P. Montagna, A.D. Libera, F. Stocchi, S. Goldwurm, J.J. Ferreira, G. Meco, E. Martignoni, L. Lopiano, L.B. Jardim, B.A. Oostra, E.R. Barbosa, Italian Parkinson Genetics Network, Bonifati, V. ATP13A2 missense mutations in juvenile parkinsonism and young onset Parkinson disease, Neurology 68 (2007) 1557–1562.
[5] J. Vallipuram, J. Grenville, D.A. Crawford, The E646D-ATP13A4 mutation associated with autism reveals a defect in calcium regulation, Cell. Mol. Neurobiol. 30 (2010) 233–246.
[6] A. Ramirez, A. Heimbach, J. Grundemann, B. Stiller, D. Hampshire, L.P. Cid, I. Goebel, A.F. Mubaidin, A.L. Wriekat, J. Roeper, A. Al-Din, A.M. Hillmer, M. Karsak, B. Liss, C.G. Woods, M.I. Behrens, C. Kubisch, Hereditary parkinsonism with dementia is caused by mutations in ATP13A2, encoding a lysosomal type 5 P-type ATPase, Nat. Genet. 38 (2006) 1184–1191.
[7] D.A. Kwasnicka-Crawford, A.R. Carson, W. Roberts, A.M. Summers, K. Rehnstrom, I. Jarvela, S.W. Scherer, Characterization of a novel cation transporter ATPase gene (ATP13A4) interrupted by 3q25-q29 inversion in an individual with language delay, Genomics 86 (2005) 182–194.
[8] M.I. Behrens, N. Brüggemann, P. Chana, P. Venegas, M. Kägi, T. Parrao, P. Orellana, C. Garrido, C.V. Rojas, J. Hauke, E. Hahnen, R. González, N. Seleme, V. Fernández, A. Schmidt, F. Binkofski, D. Kömpf, C. Kubisch, J. Hagenah, C. Klein, A. Ramirez, Clinical spectrum of Kufor–Rakeb syndrome in the Chilean kindred with ATP13A2 mutations, Mov. Disord. 25 (2010) 1929–1937, http://dx.doi.org/10.1002/mds.22996.
[9] S.A. Schneider, C. Paisan-Ruiz, N.P. Quinn, A.J. Lees, H. Houlden, J. Hardy, K.P. Bhatia, ATP13A2 mutations (PARK9) cause neurodegeneration with brain iron accumulation, Mov. Disord. 25 (2010) 979–984.
[10] A. Terman, S. Sandberg, Proteasome inhibition enhances lipofuscin formation, Ann. N. Y. Acad. Sci. 973 (2002) 309–312.
[11] T. Kurz, J.W. Eaton, U. Brunk, The role of lysosomes in iron metabolism and recycling, Int. J. Biochem. Cell Biol. 43 (2011) 1686–1697, http://dx.doi.org/10.1016/j.biocel.2011.08.016.
[12] F. de Tezanos Pinto, G.R. Corradi, H.P. Adamo, The human P5B-ATPase ATP13A2 is not a Ca^{2+} transporting pump, J. Life Sci. 5 (2011) 1–6.
[13] F. de Tezanos Pinto, G.R. Corradi, D.P. de la Hera, H.P. Adamo, CHO cells expressing the human P5-ATPase ATP13A2 are more sensitive to the toxic effects of herbicide Paraquat, Neurochem. Int. 60 (2012) 243–248.
[14] D.P. de La Hera, G.R. Corradi, H.P. Adamo, F. de Tezanos Pinto, Parkinson's disease-associated human P5B-ATPase ATP13A2 increases spermidine uptake, Biochem. J. 450 (2013) 47–53, http://dx.doi.org/10.1042/BJ20120739.
[15] U. Landegren, Measurement of cell numbers by means of the endogenous enzyme hexosaminidase. Applications to detection of lymphokines and cell surface antigens, J. Immunol. Methods 67 (1984) 379–388.
[16] J. Riemer, H.H. Hoepken, H. Czerwinska, S.R. Robinson, R. Dringen, Colorimetric ferrozine-based assay for the quantitation of iron in cultured cells, Anal. Biochem. 331 (2004) 370–375.
[17] B. Schopf, T. Neubergera, K. Schulzea, A. Petrib, M. Chastellainb, M. Hofmannc, H. Hofmannb, B. von Rechenberg, Methodology description for detection of cellular uptake of PVA coated superparamagnetic iron oxide nanoparticles (SPION) in synovial cells of sheep, J. Magn. Magn. Mater. 293 (2005) 411–418.
[18] M. Zhao, J.W. Eaton, U.T. Brunk, Protection against oxidant-mediated lysosomal rupture: a new anti-apoptotic activity of Bcl-2? FEBS Lett. 485 (2000) 104–108.
[19] D. Ramonet, A. Podhajska, K. Stafa, S. Sonnay, A. Trancikova, E. Tsika, O. Pletnikova, J.C. Troncoso, L. Glauser, D.J. Moore, PARK9-associated ATP13A2 localizes to intracellular acidic vesicles and regulates cation homeostasis and neuronal integrity, Hum. Mol. Genet. 21 (2012) 1725–1743, http://dx.doi.org/10.1093/hmg/ddr606.
[20] B. Dehay, A. Ramirez, M. Martinez-Vicente, C. Perier, M.H. Canron, E. Doudnikoff, A. Vital, M. Vila, C. Klein, E. Bezard, Loss of P-type ATPase ATP13A2/PARK9 function induces general lysosomal deficiency and leads to Parkinson disease neurodegeneration, Proc. Natl. Acad. Sci. U. S. A. 109 (2012) 9611–9616, http://dx.doi.org/10.1073/pnas.1112368109.
[21] M. Usenovic, E. Tresse, J.R. Mazzulli, J.P. Taylor, D. Krainc, Deficiency of ATP13A2 leads to lysosomal dysfunction, α-synuclein accumulation, and neurotoxicity, J. Neurosci. 32 (2012) 4240–4246, http://dx.doi.org/10.1523/JNEUROSCI.5575-11.2012.
[22] J.P. Luzio, P.R. Pryor, N.A. Bright, Lysosomes: fusion and function, Nat. Rev. Mol. Cell Biol. 8 (2007) 622–632, http://dx.doi.org/10.1038/nrm2217.
[23] T. Kurz, A. Terman, B. Gustafsson, U.T. Brunk, Lysosomes in iron metabolism, ageing and apoptosis, Histochem. Cell Biol. 129 (2008) 389–406.
[24] E.L. Eskelinen, Fine structure of the autophagosome, Methods Mol. Biol. 445 (2008) 11–28.
[25] P.M. Chen, Z.J. Gombart, J.W. Chen, Chloroquine treatment of ARPE-19 cells leads to lysosome dilation and intracellular lipid accumulation: possible implications of lysosomal dysfunction in macular degeneration, Cell Biosci. 1 (2011) 1–10, http://dx.doi.org/10.1186/2045-3701-1-10.
[26] Y.H. Yoon, K.S. Cho, J.J. Hwang, S.J. Lee, J.A. Choi, J.Y. Koh, Induction of lysosomal dilatation, arrested autophagy, and cell death by chloroquine in cultured ARPE-19 cells, Invest. Ophthalmol. Vis. Sci. 51 (2010) 6030–6037, http://dx.doi.org/10.1167/iovs.10-5278.
[27] P. Boya, G. Kroemer, Lysosomal membrane permeabilization in cell death, Oncogene 27 (2008) 6434–6451, http://dx.doi.org/10.1038/onc.2008.310.
[28] A.C. Johansson, H. Appelqvist, C. Nilsson, K. Kågedal, K. Roberg, K. Ollinger, Regulation of apoptosis-associated lysosomal membrane permeabilization, Apoptosis 15 (2010) 527–540, http://dx.doi.org/10.1007/s10495-009-0452-5.
[29] B. Halliwell, S. Chirico, Lipid peroxidation: its mechanism, measurement, and significance, Am. J. Clin. Nutr. 57 (5 Suppl) (1993) 715S–724S (discussion 724S-725S).
[30] K. Kon, J.S. Kim, A. Uchiyama, H. Jaeschke, J.J. Lemasters, Lysosomal iron mobilization and induction of the mitochondrial permeability transition in acetaminophen-induced toxicity to mouse hepatocytes, Toxicol. Sci. 117 (2010) 101–108, http://dx.doi.org/10.1093/toxsci/kfq175.
[31] Y. Lin, D.L. Epstein, P.B. Liton, Intralysosomal iron induces lysosomal membrane permeabilization and cathepsin D-mediated cell death in trabecular meshwork cells exposed to oxidative stress, Invest. Ophthalmol. Vis. Sci. 51 (2010) 6483–6495, http://dx.doi.org/10.1167/iovs.10-5410.
[32] Antunes, F., Cadenas, E. and Brunk, U.T. Apoptosis induced by exposure to a low steady-state concentration of H_2O_2 is a consequence of lysosomal rupture. Biochem. J., **356**, 549-555.
[33] B. Mirnikjoo, K. Balasubramanian, A.J. Schroit, Mobilization of lysosomal calcium regulates the externalization of phosphatidylserine during apoptosis, J. Biol. Chem. 284 (2009) 6918–6923, http://dx.doi.org/10.1074/jbc.M805288200.
[34] O. Dushek, S. Mueller, S. Soubies, D. Depoil, I. Caramalho, D. Coombs, S. Valitutti, Effects of intracellular calcium and actin cytoskeleton on TCR mobility measured by fluorescence recovery, PLoS ONE (2008)http://dx.doi.org/10.1371/journal.pone.0003913.
[35] F. Gaboriau, A. Kreder, N. Clavreul, J.P. Moulinoux, J.G. Delcros, G. Lescoat, Polyamine modulation of iron uptake in CHO cells, Biochem. Pharmacol. 67 (2004) 1629–1637.
[36] E. Løvaas, Antioxidative and metal-chelating effects of polyamines, Adv. Pharmacol. 38 (1996) 119–149.
[37] D. Soulet, B. Gagnon, S. Rivest, M. Audette, R. Poulin, A fluorescent probe of polyamine transport accumulates into intracellular acidic vesicles via a two-step mechanism, J. Biol. Chem. 279 (2004) 49355–49366.
[38] S.M. Kong, B.K. Chan, J.S. Park, K.J. Hill, J.B. Aitken, L. Cottle, H. Farghaian, A.R. Cole, P.A. Lay, C.M. Sue, A.A. Cooper, Parkinson's disease-linked human PARK9/ATP13A2 maintains zinc homeostasis and promotes α-Synuclein externalization via exosomes, Hum. Mol. Genet. 23 (2014) 2816–2833, http://dx.doi.org/10.1093/hmg/ddu099.
[39] M.R. Marzabadi, E. Løvaas, Spermine prevent iron accumulation and depress lipofuscin accumulation in cultured myocardial cells, Free Radic. Biol. Med. 21 (1996) 375–381.
[40] U.T. Brunk, A. Terman, The mitochondrial-lysosomal axis theory of aging: accumulation of damaged mitochondria as a result of imperfect autophagocytosis, Eur. J. Biochem. 269 (2002) 1996–2002.
[41] J. Bras, A. Verloes, S.A. Schneider, S.E. Mole, R.J. Guerreiro, Mutation of the parkinsonism gene ATP13A2 causes neuronal ceroid-lipofuscinosis, Hum. Mol. Genet. 21 (2012) 2646–2650, http://dx.doi.org/10.1093/hmg/dds089.
[42] P.J. Schultheis, S.M. Fleming, A.K. Clippinger, J. Lewis, T. Tsunemi, B. Giasson, D.W. Dickson, J.R. Mazzulli, M.E. Bardgett, K.L. Haik, O. Ekhator, A.K. Chava, J. Howard, M. Gannon, E. Hoffman, Y. Chen, V. Prasad, S.C. Linn, R.J. Tamargo, W. Westbroek, E. Sidransky, D. Krainc, G.E. Shull, Atp13a2-deficient mice exhibit neuronal ceroid lipofuscinosis, limited α-synuclein accumulation and age-dependent sensorimotor deficits, Hum. Mol. Genet. 22 (2013) 2067–2082, http://dx.doi.org/10.1093/hmg/ddt057.
[43] S.R. Cronin, R. Rao, R.Y. Hampton, Cod1p/Spf1p is a P-type ATPase involved in ER function and Ca^{2+} homeostasis, J. Cell Biol. 157 (2002) 1017–1028.
[44] K. Schmidt, D.M. Wolfe, B. Stiller, D.A. Pearce, Cd^{2+}, Mn^{2+}, Ni^{2+} and Se^{2+} toxicity to *Saccharomyces cerevisiae* lacking YPK9p the orthologue of human ATP13A2, Biochem. Biophys. Res. Commun. 383 (2009) 198–202.
[45] A.D. Gitler, A. Chesi, M.L. Geddie, K.E. Strathearn, S. Hamamichi, K.J. Hill, K.A. Caldwell, G.A. Caldwell, A.A. Cooper, J.C. Rochet, S. Lindquist, Alpha-synuclein is part of a diverse and highly conserved interaction network that includes PARK9 and manganese toxicity, Nat. Genet. 41 (2009) 308–315.
[46] J. Tan, T. Zhang, L. Jiang, J. Chi, D. Hu, Q. Pan, D. Wang, Z. Zhang, Regulation of intracellular manganese hemeostasis by Kufor–Rakeb syndrome associated ATP13A2, J. Biol. Chem. 286 (2011) 29654–29662.
[47] J.P. Covy, E.A. Waxman, B.I. Giasson, Characterization of cellular protective effects of ATP13A2/PARK9 expression and alterations resulting from pathogenic mutants, J. Neurosci. Res. 90 (2012) 2306–2316, http://dx.doi.org/10.1002/jnr.23112.
[48] J.S. Park, B. Koentjoro, D. Veivers, A. Mackay-Sim, C.M. Sue, Parkinson's disease-associated human ATP13A2 (PARK9) deficiency causes zinc dyshomeostasis and mitochondrial dysfunction, Hum. Mol. Genet. 23 (2014) 2802–2815, http://dx.doi.org/10.1093/hmg/ddt623.
[49] D.T. Dexter, A. Carayon, F. Javoy-Agid, Y. Agid, F.R. Wells, S.E. Daniel, A.J. Lees, P. Jenner, C.D. Marsden, Alterations in the levels of iron, ferritin and other trace metals in Parkinson's disease and other neurodegenerative diseases affecting the basa ganglia, Brain 114 (1991) 1953–1975.
[50] I. Hozumi, T. Hasegawa, A. Honda, K. Ozawa, Y. Hayashi, K. Hashimoto, M. Yamada, A. Koumura, T. Sakurai, A. Kimura, Patterns of levels of biological metals in CSF differ among neurodegenerative diseases, J. Neurol. Sci. 303 (2011) 95–99.
[51] F.J. Jiménez-Jiménez, P. Fernández-Calle, M. Martínez-Vanaclocha, E. Herrero, J. Molina, A. Vázquez, R. Codoceo, Serum levels of zinc and copper in patients with Parkinson's disease, J. Neurol. Sci. 112 (1992) 30–33.
[52] A.H.V. Schapira, Calcium dysregulation in Parkinson's disease, Brain 136 (2013) 2015–2016.

[53] M. Aschner, K.M. Erikson, E. Herrero Hernández, R. Tjalkens, Manganese and its role in Parkinson's disease: from transport to neuropathology, Neruomol. Med. 11 (2009) 252–266, http://dx.doi.org/10.1007/s12017-009-8083-0.
[54] A. Catala, Lipid peroxidation modifies the picture of membranes from the "Fluid Mosaic Model" to the "Lipid Whisker Model", Biochimie 94 (2012) 101–109.
[55] T.R. Graham, Flippases and vesicle-mediated protein transport, Trends Cell Biol. 14 (2004) 670–677.
[56] S. vanVeen, D.M. Sørensen, T. Holemans, H.W. Holen, M.G. Palmgren, P. Vangheluwe, Cellular function and pathological role of ATP13A2 and related P-type transport ATPases in Parkinson's disease and other neurological disorders, Front. Mol. Neurosci. 7 (48) (2014)http://dx.doi.org/10.3389/fnmol.2014.00048.
[57] X. Fan, G. Luo, D. Yang, M. Ming, H. Liu, P. Pu, W. Le, Critical role of lysosome and its associated protein cathepsin D in manganese-induced toxicity in cultured midbrain astrocyte, Neurochem. Int. 56 (2010) 291–300, http://dx.doi.org/10.1016/j.neuint.2009.11.001.
[58] J.J. Hwang, S.J. Lee, T.Y. Kim, J.H. Cho, J.Y. Koh, Zinc and 4-hydroxy-2-nonenal mediate lysosomal membrane permeabilization induced by H_2O_2 in cultured hippocampal neurons, J. Neurosci. 28 (2008) 3114–3122, http://dx.doi.org/10.1523/JNEUROSCI.0199-08.2008.